

Self-Adaptive Reconfigurable Arrays (SARA): Using ML to Assist Scaling GEMM Acceleration

Ananda Samajdar

Georgia Tech

Atlanta, GA

anandsamajdar@gatech.edu

Michael Pellauer

NVIDIA

Boston, MA

mpellauer@nvidia.com

Tushar Krishna

Georgia Tech

Atlanta, GA

tushar@ece.gatech.edu

Abstract—With increasing diversity in Deep Neural Network (DNN) models in terms of layer shapes and sizes, the research community has been investigating flexible/reconfigurable accelerator substrates. This line of research has opened up two challenges. The first is to determine the appropriate amount of flexibility within an accelerator array that can trade-off the performance benefits versus the area overheads of the reconfigurability. The second is being able to determine the right configuration of the array for the current DNN model and/or layer and reconfigure the accelerator at runtime.

This work introduces a new class of accelerators that we call *Self Adaptive Reconfigurable Array (SARA)*. SARA architectures comprise of both a reconfigurable array and a hardware unit capable of determining an optimized configuration for the array at runtime. We demonstrate an instance of SARA with an accelerator we call *SAGAR* that introduces a novel reconfigurable systolic array that can be configured to work as a distributed collection of smaller arrays of various sizes or as a single array with flexible aspect ratios. We also develop a novel recommendation neural network called *ADAPTNET* which recommends an array configuration and dataflow for the current layer parameters. An integrated custom hardware *ADAPTNETX* runs *ADAPTNET* at runtime and reconfigures the array, making the entire accelerator self sufficient. *SAGAR* is capable of providing the same mapping flexibility as a collection of 1024 4×4 arrays working as a distributed system while achieving 3.5 \times more power efficiency and 3.2 \times higher compute density. Furthermore, when tested over 2×10^5 cases, the runtimes (GeoMean) achieved on the recommended parameters from *ADAPTNET* is 99.93% of the best achievable runtime.

I. INTRODUCTION

General Matrix to Matrix Multiplication (GEMMs) is at the heart of Deep Neural Network (DNN) training and inference and thus has been the target application of many accelerator designs [4], [7], [8], [9], [13], [37]. However these individual devices work on small matrix tiles, and do not have enough computation power to work on larger networks without multiple costly passes. Recent proposals [9] [35] have demonstrated the need for scaling the DNN computation engines to meet the computation demands of contemporary workloads. Despite extensive research and product development on architectures for small-tile GEMMs, designing efficient architectures for performing GEMMs at scale is still non-trivial.

The crux of the problem is that there exists a pernicious trade-off between *scalability* and *utilization* (or mapping efficiency). Scalability is a direct consequence of simplicity and regularity of a particular design. For instance, regular designs like the TPU [13] (systolic array) can pack large number of MAC units

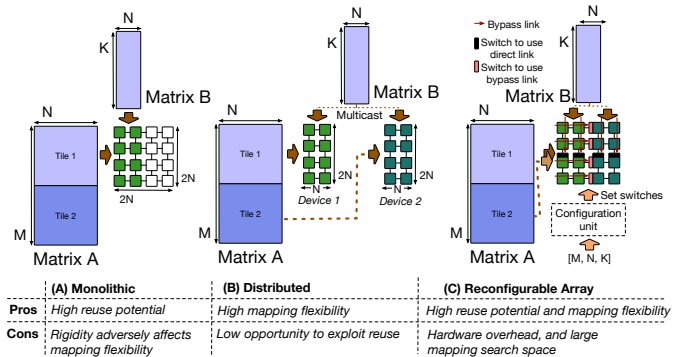


Fig. 1. Challenges in efficiently scaling GEMM arrays.

(256×256) in a reasonable power and area budget. While a flexible design like SIGMA [28] increases implementation cost to buy flexibility. Given that irregular workload dimensions are more of a norm than exception [28], this cost seems to be a necessary evil. However, a recent study [32] argues that a distributed *scaled out*¹ setting is a feasible alternative to gain flexibility, which is further corroborated by recent architecture proposals [9], [35].

Figure 1 provides intuition on why scale-out is more performant than scale-up. Both the monolithic and distributed accelerators have the same number of MAC units ($4N^2$), and are executing the same workload ($MatA \times MatB$). While the distributed accelerator (Figure 1(b)) can map the entire computation in a single step, the monolithic configuration (Figure 1(a)) needs two. The irregular size of the workloads and the mapping rigidity of the monolithic configuration are responsible for the serialization, even when compute resources are available.

Unfortunately, scaling out compromises on operand reuse and thus energy efficiency. First, spatial reuse via wires is limited since communication paths between two distinct compute units are fundamentally lower-bandwidth than within the array—in the worst case requiring off-chip access [35]. As a corollary therefore, each compute unit needs to have their own separate locally-placed high-bandwidth memory to store operand data. These individual memories are smaller than the aggregate memory available in a scaled-up system, and thus less able to exploit temporal reuse. To make matters worse, some data

¹We use scale-up/scale-out interchangeably with monolithic/distributed.

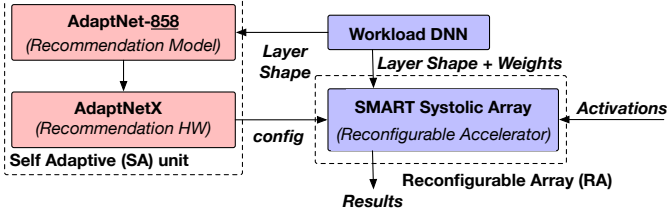


Fig. 2. The constitution and interactions of the self adaptive (SA) and reconfigurable array (RA) components to make up the SARA accelerator called *SAGAR* in this work.

operands must be replicated, reducing capacity even further.

Contribution 1: In this paper, we propose a novel accelerator micro-architecture organization called SMARTSYSTOLIC Array (SSA) aimed to attain the benefits of monolithic (i.e., scale-up) and distributed (i.e., scale-out) designs for efficient GEMM computation in a single unified substrate. We choose systolic arrays as our scale-up building blocks, since the simplicity of these arrays leads to low area and power overheads, maximizing local bandwidth while minimizing communication distance. To mitigate the under-utilization problem, we propose augmenting the traditional systolic design with a bypass interconnection network inspired by SMART [17]. These links permits us to emulate similar mapping to a distributed cluster of accelerator, within a monolithic compute array (Figure 1(c)). The SMART-like links are configurable, and can therefore emulate distributed systems of different granularities, eg. a system with 128×128 MAC (multiply and accumulate units) can be configured to be used as $4 \times 64 \times 64$ units or $16 \times 32 \times 32$ units or even $32 \times 32 \times 16$ units.

Contribution 2: Finding the optimal configuration for such a reconfigurable array is the key to achieve the best performance. However, the best configuration depends on the workload, which means the configuration needs to be determined at runtime. A finer granularity of reconfiguration improves mapping efficiency, but at the same time increases the configuration search space [15], [27]. Extra resources are needed to ensure that configuration search does not become a bottleneck at runtime. We develop a novel light weight neural recommendation model called ADAPTNET, which replaces costly configuration search with constant time inference operation at runtime. For a given workload dimension, the network recommends best architecture configuration as well as the mapping (dataflow) strategy. The recommended configurations attain about 99.93% of the best runtime on average (GeoMean) in our tests with 200K samples.

Contribution 3: We also design a custom hardware for running ADAPTNET, called ADAPTNETX, and augment it with the reconfigurable accelerator. The resulting design is thus self sufficient for providing optimal performance without external inputs.

Contribution 4: We integrate these three components into an accelerator which we call ‘Shape Adaptive GEMM AcceleratoR (*SAGAR*)²’ as shown in Figure 2 and evaluate

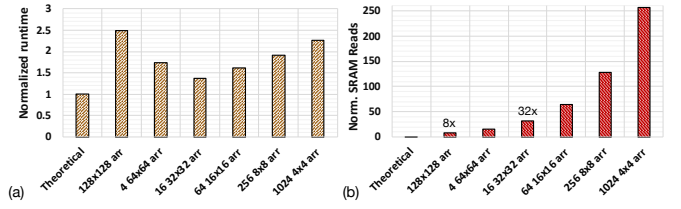


Fig. 3. The trade-off between improved runtime and lost operand reuse in compute equivalent monolithic and distributed systolic array configurations. Subfigures show (a) the theoretical minimum runtime, and the runtime obtained for stall free operation of monolithic and compute normalized distributed systolic array settings; and (b) the corresponding SRAM reads, normalized to theoretical minimum reads required when multiplying a 256×64 matrix with another 64×256 matrix.

its performance across various configurations. We show that *SAGAR* has 3.2 \times higher compute density and 3.5 \times improved power efficiency, over equivalent scaled-out systolic array. The extra flexibility costs <10% in area and 50% in power, compared to equivalent scaled-up systolic array. Compared to an area normalized state-of-the-art flexible scalable accelerator [28], *SAGAR* incorporates 45% more compute, while when comparing compute-equivalent configurations, *SAGAR* consumes 43% less power and saves 30% area footprint (see Section VI-B).

We believe our proposed accelerator is the first in a class of designs we name *Self Adaptive Reconfigurable Array (SARA)* (Figure 2). To summarize, we make the following contributions. (i) We propose **SSA**, a reconfigurable architecture for scalable GEMM acceleration, simultaneously achieving high utilization and reuse. (ii) We develop **ADAPTNET**, a lean recommendation neural net which suggests optimized configuration and dataflow with high accuracy. (iii) We implement **ADAPTNETX**, a hardware capable of running **ADAPTNET** in constant time and configuring **SSA** at runtime. (iv) We integrate the above components into a *SARA* accelerator called ***SAGAR***, which achieves optimal runtime at lower power and area than state of the art.

II. BACKGROUND AND MOTIVATION

A. Scaling DNN acceleration

Google’s Tensor Processing Unit(TPU) [13], a large 256×256 systolic array based accelerator, is one of the first data-center class DNN accelerators. However, as the authors report, irregular sized GEMM operations found in recurrent workloads, result in as much as 86% under-utilization of the array, attributed to the rigidity of mapping. A recent accelerator proposal called SIGMA [28] tries to alleviate this problem by introducing flexibility of mapping by using a two level interconnect to deliver data to the computation elements. On the other hand recent proposals like Simba [35] take the scaled-out approach by building a cluster of Multi Chip Modules (MCMs) to increase the compute capability of the design. Tangram [9] on the other hand proposes a scaled-out design where the problems of data replication is potentially mitigated by communicating over an interconnection network and precisely timing the communication and compute.

²Sagar is a Sanskrit word that means Ocean, reflecting the ability of our accelerator to have flexible shapes

While recent research targets both scaled-up and scaled-out approach, it is not immediately clear if one design direction has an immediate advantage over the other. One study [32] argues that for systolic array based designs, scaled-out configuration is almost always better than scaled-out in terms of performance. However this benefit comes at a cost of huge increase in external bandwidth requirement (in this case from DRAM), which renders implementing such a design impractical at scale.

To help understand the trade offs involved in choosing a performant configuration, and the associated loss of reuse we perform a simple experiment. We run one GEMM operation, involving operand matrices of sizes sizes 256×64 and 64×256 on various systolic array configurations. These are, a 128×128 monolithic array, and five distributed scale-out configurations viz. 4 64×64 arrays, 16 32×32 arrays, 64 16×16 arrays, 256 8×8 arrays, and 1024 4×4 arrays. We obtain the runtime and memory accesses for running this workload on all the array configurations using SCALE-Sim [33] (see Section VI-A). In Figure 3(a) we show the runtime normalized to the theoretical minimum cycles required. Please note that with the chosen matrix dimensions, the systolic arrays in all the configurations are mapped 100% with useful computation. The differences in runtime arise from serialization and pipeline filling latency. We observe that the configuration with 32×32 array is the most performant beating the the monolithic configuration by about $2 \times$. In Figure 3(b) we depict the SRAM read accesses performed by all the array configurations, normalized to the theoretical minimum number of reads possible. From this figure we observe that the 32×32 configuration performed about $4 \times$ more memory accesses then the monolithic. The excess memory accesses, which lead to reduced energy efficiency, result from the loss of wire reuse as compared to a monolithic array.

From the discussion above we make two observations.

(i) Distributed arrays are more performant than an equivalent monolithic array, even when mapping efficiency is 100% on both. However, the optimal size of each device in a distributed setting is workload dependent. (ii) Monolithic configurations are strictly more energy efficient than distributed arrays, due to loss the of spatio-temporal reuse in the latter.

Mitigating the loss of reuse in a distributed setting is therefore the key to achieve both performance and energy efficiency simultaneously and therefore is the goal of this work.

B. Single cycle multi-hop links with SMART

SMART [17] describe a mechanism to reduce the average hop count of network on chip (NoC) by introducing bypass paths which could be used to allow multi-hop traversal of a packet within a cycle. The hardware changes needed to implement the proposed scheme involve two changes. First is the addition of an alternate path from the input ports of each router to the input selector mux bypassing the queuing buffer in the datapath. Second is addition dedicated control paths from each router to HPC_{max} (maximum possible hops per cycle) routers in the downstream at every direction.

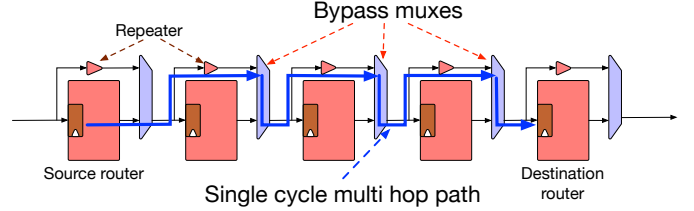


Fig. 4. Multi-hop traversals in a single cycle using SMART [17]

The mechanism to use the bypassing path happens in two steps. In the first step, the SMART path is setup by the source router, one cycle prior to the actual movement of the packet. The source router broadcasts the SMART Setup Request (SSR) to the downstream routers by sending a SSR over dedicated SSR links. Each SSR link is $\log_2(HPC_{max})$ bit wide and indicates the number of hops the flit wants to go. The request precludes the flit by one cycle, which allows the downstream routers make the decision of accepting the packet before it is launched. The downstream routers employ a fixed priority scheme to ensure that there are no packet drops.

C. Recommendation Systems

Recommendation systems are widely used on social media, streaming services, online marketplaces etc. to show most relevant advertisements or products for a given user to increase the click-through rate and provide meaningful personalized content. Over the years neural networks have consistently provided improved performance over then state of the methods like Neural collaborative filtering (NCF) [12] over collaborative filtering [34] and Neural factorization machine(NFM) [11] over factorization machine [30]. The current state of the art method called the Deep Learning Recommendation Model (DLRM) [24] uses the techniques like feature embeddings and feature interactions employed NCF and NFM, coupled with deep multi layer perceptrons. In the DLRM architecture, a combination of sparse and dense features are used as inputs. The sparse features are converted into dense vectors in a learned latent space via embedding lookup. The resulting dense features are then passed through multiple dense layers followed by feature interactions [11], [24]. Finally, the combined features are send through a few more dense layers to get the final classification.

III. RECONFIGURABLE ARRAY ARCHITECTURE

We augment a base monolithic systolic array with additional bypass paths along the row and columns, inspired by SMART [17]. This enables us to realize a flexible, energy efficient design which can be configured to act as a large single array (i.e., scale-up) or a collection of smaller arrays (i.e., scale-out), whenever required.

A. Compute array

Traditional MAC units. In Figure 5(a) we show a traditional systolic array constructed by laying down Multiply-and-Accumulate (MAC) (Figure 5(b)) units in a 2D grid. Each MAC unit is designed to get an operand from either both (*Left in, Top in*) ports or from either of the ports, and perform

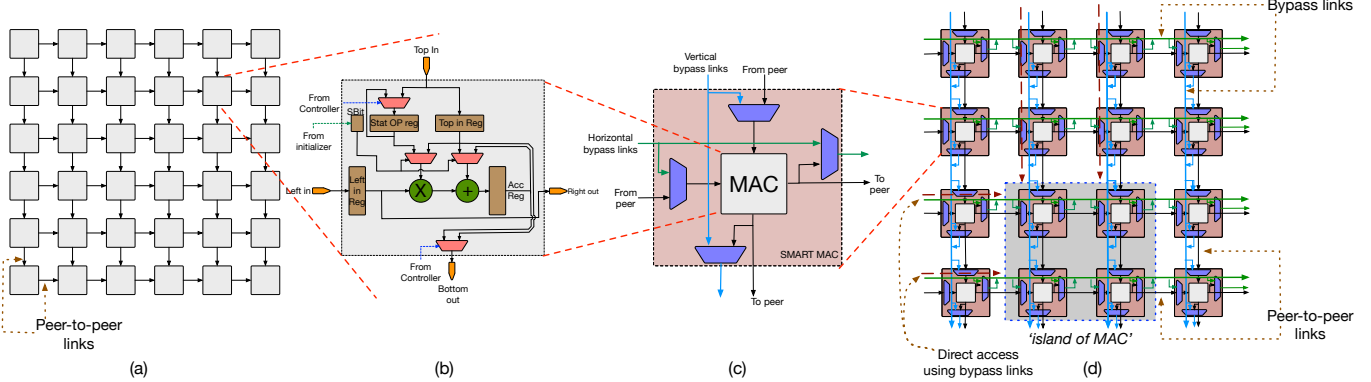


Fig. 5. (a) A systolic array of traditional MAC units, (b) the architecture of a traditional MAC unit, (c) addition of bypass paths to a traditional MAC to create a SMART MAC unit to (d) enable flexible mapping in a systolic array by creating ‘islands’ of MAC units capable of receiving data directly from SRAM banks by bypassing its peers

multiplication and addition operation. In the next cycle the operand data received is sent to its neighbour over the peer-to-peer links. The internal registers, and multiplexers enable the array to work in output stationary (OS), weight stationary (WS), and input stationary operations (IS) [4]. This simple mechanism of data movement results in high wire reuse, but at the same time restricts the mapping of compute only to those operations which require same set of operands to be mapped along a row or a column.

SMART MAC units. Any mechanism to enable MAC units to accept data from sources other than the neighbouring MAC unit will ease the restrictions of mapping compute and therefore enable high utilization. In Figure 5(c) we depict a modified MAC unit, which is augmented with multiplexers in the input and output ports. *We call this, a SMART MAC unit.* Note that SMART MAC denotes a MAC unit with multiplexers on one or more input/output ports to enable bypass, not necessarily on all ports. These multiplexers enable reading and writing to wires other than the peer-to-peer links, thus enabling it to receive and work on operands unrelated to the ones forwarded by its peers. Akin to the multi-hop bypass path employed in the SMART-NoC, we can allocate bypass busses from memory to the array, to provide extra channels to move data. Connecting one of the inputs of the multiplexers with these bypass busses from memory therefore enables us to create ‘islands’ of MAC units. These ‘islands’ are a collection of neighbouring MAC units forming a rectangular group which can act as independent smaller arrays. We can map computations on such ‘islands’ independent of the other neighbouring MACs which translates to improved mapping flexibility (see Figure 5(d)). However, note that this design allows for arbitrary reconfiguration which is an overkill and makes the design costlier than necessary.

Systolic Cells. We find that an alternative design, employing a mix of traditional MAC units (Figure 5(b)) and the SMART MAC units to be a more practical choice. Instead of allowing flexible connectivity at the granularity of individual MAC units, we provide reconfigurability at the scale of a smaller array by allowing flexible connectivity at the edge of the said sub-array. For example, in Figure 6(a) we show a 4x4 sub-array so

designed. We refer to these sub-arrays as *systolic-cells*. As can be observed in Figure 6(a), a *systolic-cell* is constructed by using SMART MAC units in the edge of the array, and traditional MAC units (Figure 6(b)) in the inside, and then connecting them using peer-to-peer links. This helps reduce implementation cost in three ways. First, the number of SMART MAC used in the array is reduced. Second, in the remaining SMART MAC, multiplexers are not required on each port, instead only the ports which communicate with MACs outside the given *systolic-cell* need multiplexers to read and write data to the bypass links. Third, the number of bypass links are also reduced as a consequence of reduction in the number of multiplexers. With this optimization the bypasses are now performed at the granularities of the *systolic-cells*.

Scale-up and Scale-out using Systolic Cells. Larger arrays can be created by arranging and connecting the *systolic-cells* as depicted in Figure 6(b) using the peer-to-peer links. At the edge of each *systolic-cell* the bypass paths can be connected to the bypass links. Please note that dedicated bypass links are allocated to each *systolic-cell* to allow concurrency. Attaining flexible mapping in such a design is a matter of configuring the multiplexers of the *systolic-cells*. Depending on the mapping requirement an user can chose not to use the bypass paths at all and use the entire array as a single monolithic unit, by setting the multiplexers to accept data only to/from the peer-to-peer links, (this is the case depicted in Figure 6(b)), which is equivalent to a *scaled-up* configuration. On the other hand, the user can set all the multiplexers to accept and deliver data solely to the bypass links, therefore operating as a cluster of arrays, each the size of a *systolic-cell*. This configuration, depicted in Figure 6(c) is equivalent to a *scaled-out* configuration. Other scaled-out configurations with sub arrays larger than the *systolic-cell* size is also possible to be realized by logically combining a few *systolic-cells* by setting some of multiplexers to connect with the bypass links and others to connect with the peer-to-peer links. The availability of such variety of choices for reconfiguration leads to flexible and efficient mapping, hence improving the utilization and energy efficiency of the design. Note that unlike the SMART

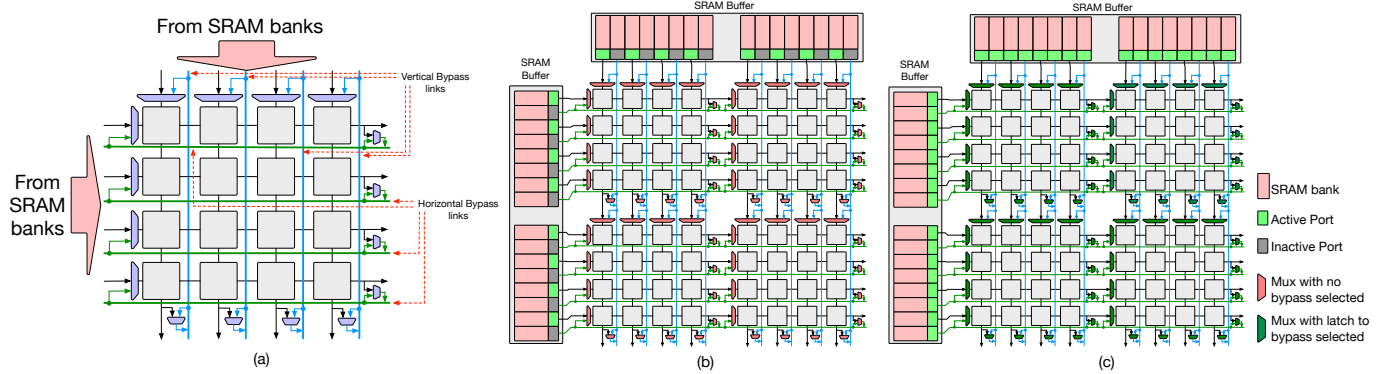


Fig. 6. (a) Construction of a 4×4 *systolic-cell* with bypass muxes and bypass links. (b) A 8×8 SMART systolic array operating in scale-up configuration. Each 4×4 *systolic-cell* is connected to its neighbor with the peer-to-peer links as the bypass muxes are turned off. The SRAM ports connected to bypass links are unused. (c) Configuration of bypass muxes to enable the 8×8 SMART systolic array to work as a scaled-out distributed collection of systolic arrays. The bypass muxes are turned on to allow *systolic-cells* to directly connect to the SRAM ports which are all active.

NoC [17], these muxes are configured statically, and hence do not need to worry about arbitration.

B. Scratch pad memory

The array constructed from *systolic-cells* are backed by SRAM scratchpad memory, which are constructed as two individual buffers. Each of these buffers is dedicated to one of the operand matrices. Such scratchpad SRAM buffers are common in accelerators, and are designed to reduce the number of off chip accesses and facilitate temporal reuse. Each operand buffer is operated in a double buffered fashion, so that the pre-fetch latency can be minimized. The system also comprises of a third buffer which is used to store generated output elements.

Unlike conventional accelerators however, our systolic *systolic-cell* based design has bypass links, which are also needed to be backed by the memory. We provision for this extra bandwidth by increasing the number of memory banks in the scratchpad SRAM buffers. In a traditional systolic array based design, each row and column of the array is connected to one dedicated SRAM port to supply one element per cycle each. In a similar fashion we allocate one port for each row, column and the individual bypass links. To reduce the complexity of multiplexing data within the SRAM, we increase the number of SRAM banks to support the increased number of ports. For example, the compute arrays shown in Figure 6(c) is backed by two scratchpad memories each with 16 ports and would be constructed as collection of 16 SRAM banks. The SRAM banks in a traditional $8 \times$ systolic array on the other hand would have 8 port per buffer; one per each row/column. We evaluate the overheads for such a design in Section VI-B.

Despite having the same number of SRAM ports as in a distributed configuration, this approach has a couple of advantages over the latter. *First*, there is no replication of data required, which otherwise reduces the effective capacity of the system therefore adversely affecting reuse. In our design by eliminating replication we inherently improve the temporal reuse of operands. *Second*, each of the *systolic-cells* can access data in the entire operand buffer. Due to unified memory control of each buffer, operation like multi-cast are implicit in form

```

1  input allLayerParameters
2  input numLayers
3
4  for i in (0:numLayers):
5      layerParameter = allLayerParameters[i]
6
7      numPartition,
8      rowPerPartition, colPerPartition, dataflow
9      = recNetInference(layerParameter)
10
11  setBypassMuxes( numPartition,
12                  rowPerPartition,
13                  colPerPartition)
14
15
16
17
18
19
20
21
22
23
24
25
26
27
28
29
30
31
32
33
34
35
36
37
38
39
40
41
42
43
44
45
46
47
48
49
50
51
52
53
54
55
56
57
58
59
60
61
62
63
64
65
66
67
68
69
70
71
72
73
74
75
76
77
78
79
80
81
82
83
84
85
86
87
88
89
90
91
92
93
94
95
96
97
98
99
100
101
102
103
104
105
106
107
108
109
110
111
112
113
114
115
116
117
118
119
120
121
122
123
124
125
126
127
128
129
130
131
132
133
134
135
136
137
138
139
140
141
142
143
144
145
146
147
148
149
150
151
152
153
154
155
156
157
158
159
160
161
162
163
164
165
166
167
168
169
170
171
172
173
174
175
176
177
178
179
180
181
182
183
184
185
186
187
188
189
190
191
192
193
194
195
196
197
198
199
200
201
202
203
204
205
206
207
208
209
210
211
212
213
214
215
216
217
218
219
220
221
222
223
224
225
226
227
228
229
230
231
232
233
234
235
236
237
238
239
240
241
242
243
244
245
246
247
248
249
250
251
252
253
254
255
256
257
258
259
259
260
261
262
263
264
265
266
267
268
269
270
271
272
273
274
275
276
277
278
279
279
280
281
282
283
284
285
286
287
288
289
289
290
291
292
293
294
295
296
297
298
299
299
300
301
302
303
304
305
306
307
308
309
309
310
311
312
313
314
315
316
317
318
319
319
320
321
322
323
324
325
326
327
328
329
329
330
331
332
333
334
335
336
337
338
339
339
340
341
342
343
344
345
346
347
348
349
349
350
351
352
353
354
355
356
357
358
359
359
360
361
362
363
364
365
366
367
368
369
369
370
371
372
373
374
375
376
377
378
379
379
380
381
382
383
384
385
386
387
388
389
389
390
391
392
393
394
395
396
397
398
399
399
400
401
402
403
404
405
406
407
408
409
409
410
411
412
413
414
415
416
417
418
419
419
420
421
422
423
424
425
426
427
428
429
429
430
431
432
433
434
435
436
437
438
439
439
440
441
442
443
444
445
446
447
448
449
449
450
451
452
453
454
455
456
457
458
459
459
460
461
462
463
464
465
466
467
468
469
469
470
471
472
473
474
475
476
477
478
479
479
480
481
482
483
484
485
486
487
488
489
489
490
491
492
493
494
495
496
497
498
499
499
500
501
502
503
504
505
506
507
508
509
509
510
511
512
513
514
515
516
517
518
519
519
520
521
522
523
524
525
526
527
528
529
529
530
531
532
533
534
535
536
537
538
539
539
540
541
542
543
544
545
546
547
548
549
549
550
551
552
553
554
555
556
557
558
559
559
560
561
562
563
564
565
566
567
568
569
569
570
571
572
573
574
575
576
577
578
579
579
580
581
582
583
584
585
586
587
588
589
589
590
591
592
593
594
595
596
597
597
598
599
599
600
601
602
603
604
605
606
607
608
609
609
610
611
612
613
614
615
616
617
618
618
619
620
621
622
623
624
625
626
627
628
629
629
630
631
632
633
634
635
636
637
638
639
639
640
641
642
643
644
645
646
647
648
649
649
650
651
652
653
654
655
656
657
658
659
659
660
661
662
663
664
665
666
667
668
669
669
670
671
672
673
674
675
676
677
678
678
679
680
681
682
683
684
685
686
687
687
688
689
689
690
691
692
693
694
695
696
696
697
698
699
699
700
701
702
703
704
705
706
707
708
709
709
710
711
712
713
714
715
716
716
717
718
719
719
720
721
722
723
724
725
726
727
727
728
729
730
731
732
733
734
735
736
737
737
738
739
740
741
742
743
744
745
745
746
747
748
749
749
750
751
752
753
754
755
756
757
757
758
759
759
760
761
762
763
764
765
766
766
767
768
769
769
769
770
771
772
773
774
775
775
776
777
777
778
779
779
779
780
781
782
783
784
785
785
786
787
787
787
788
789
789
789
789
790
791
792
792
792
793
793
793
793
794
794
794
794
795
795
795
795
796
796
796
796
797
797
797
797
798
798
798
798
799
799
799
799
800
800
800
800
801
801
801
801
802
802
802
802
803
803
803
803
804
804
804
804
805
805
805
805
806
806
806
806
807
807
807
807
808
808
808
808
809
809
809
809
810
810
810
810
811
811
811
811
812
812
812
812
813
813
813
813
814
814
814
814
815
815
815
815
816
816
816
816
817
817
817
817
818
818
818
818
819
819
819
819
820
820
820
820
821
821
821
821
822
822
822
822
823
823
823
823
824
824
824
824
825
825
825
825
826
826
826
826
827
827
827
827
828
828
828
828
829
829
829
829
830
830
830
830
831
831
831
831
832
832
832
832
833
833
833
833
834
834
834
834
835
835
835
835
836
836
836
836
837
837
837
837
838
838
838
838
839
839
839
839
840
840
840
840
841
841
841
841
842
842
842
842
843
843
843
843
844
844
844
844
845
845
845
845
846
846
846
846
847
847
847
847
848
848
848
848
849
849
849
849
850
850
850
850
851
851
851
851
852
852
852
852
853
853
853
853
854
854
854
854
855
855
855
855
856
856
856
856
857
857
857
857
858
858
858
858
859
859
859
859
860
860
860
860
861
861
861
861
862
862
862
862
863
863
863
863
864
864
864
864
865
865
865
865
866
866
866
866
867
867
867
867
868
868
868
868
869
869
869
869
870
870
870
870
871
871
871
871
872
872
872
872
873
873
873
873
874
874
874
874
875
875
875
875
876
876
876
876
877
877
877
877
878
878
878
878
879
879
879
879
880
880
880
880
881
881
881
881
882
882
882
882
883
883
883
883
884
884
884
884
885
885
885
885
886
886
886
886
887
887
887
887
888
888
888
888
889
889
889
889
890
890
890
890
891
891
891
891
892
892
892
892
893
893
893
893
894
894
894
894
895
895
895
895
896
896
896
896
897
897
897
897
898
898
898
898
899
899
899
899
900
900
900
900
901
901
901
901
902
902
902
902
903
903
903
903
904
904
904
904
905
905
905
905
906
906
906
906
907
907
907
907
908
908
908
908
909
909
909
909
910
910
910
910
911
911
911
911
912
912
912
912
913
913
913
913
914
914
914
914
915
915
915
915
916
916
916
916
917
917
917
917
918
918
918
918
919
919
919
919
920
920
920
920
921
921
921
921
922
922
922
922
923
923
923
923
924
924
924
924
925
925
925
925
926
926
926
926
927
927
927
927
928
928
928
928
929
929
929
929
930
930
930
930
931
931
931
931
932
932
932
932
933
933
933
933
934
934
934
934
935
935
935
935
936
936
936
936
937
937
937
937
938
938
938
938
939
939
939
939
940
940
940
940
941
941
941
941
942
942
942
942
943
943
943
943
944
944
944
944
945
945
945
945
946
946
946
946
947
947
947
947
948
948
948
948
949
949
949
949
950
950
950
950
951
951
951
951
952
952
952
952
953
953
953
953
954
954
954
954
955
955
955
955
956
956
956
956
957
957
957
957
958
958
958
958
959
959
959
959
960
960
960
960
961
961
961
961
962
962
962
962
963
963
963
963
964
964
964
964
965
965
965
965
966
966
966
966
967
967
967
967
968
968
968
968
969
969
969
969
970
970
970
970
971
971
971
971
972
972
972
972
973
973
973
973
974
974
974
974
975
975
975
975
976
976
976
976
977
977
977
977
978
978
978
978
979
979
979
979
980
980
980
980
981
981
981
981
982
982
982
982
983
983
983
983
984
984
984
984
985
985
985
985
986
986
986
986
987
987
987
987
988
988
988
988
989
989
989
989
990
990
990
990
991
991
991
991
992
992
992
992
993
993
993
993
994
994
994
994
995
995
995
995
996
996
996
996
997
997
997
997
998
998
998
998
999
999
999
999
1000
1000
1000
1000
1001
1001
1001
1001
1002
1002
1002
1002
1003
1003
1003
1003
1004
1004
1004
1004
1005
1005
1005
1005
1006
1006
1006
1006
1007
1007
1007
1007
1008
1008
1008
1008
1009
1009
1009
1009
1010
1010
1010
1010
1011
1011
1011
1011
1012
1012
1012
1012
1013
1013
1013
1013
1014
1014
1014
1014
1015
1015
1015
1015
1016
1016
1016
1016
1017
1017
1017
1017
1018
1018
1018
1018
1019
1019
1019
1019
1020
1020
1020
1020
1021
1021
1021
1021
1022
1022
1022
1022
1023
1023
1023
1023
1024
1024
1024
1024
1025
1025
1025
1025
1026
1026
1026
1026
1027
1027
1027
1027
1028
1028
1028
1028
1029
1029
1029
1029
1030
1030
1030
1030
1031
1031
1031
1031
1032
1032
1032
1032
1033
1033
1033
1033
1034
1034
1034
1034
1035
1035
1035
1035
1036
1036
1036
1036
1037
1037
1037
1037
1038
1038
1038
1038
1039
1039
1039
1039
1040
1040
1040
1040
1041
1041
1041
1041
1042
1042
1042
1042
1043
1043
1043
1043
1044
1044
1044
1044
1045
1045
1045
1045
1046
1046
1046
1046
1047
1047
1047
1047
1048
1048
1048
1048
1049
1049
1049
1049
1050
1050
1050
1050
1051
1051
1051
1051
1052
1052
1052
1052
1053
1053
1053
1053
1054
1054
1054
1054
1055
1055
1055
1055
1056
1056
1056
1056
1057
1057
1057
1057
1058
1058
1058
1058
1059
1059
1059
1059
1060
1060
1060
1060
1061
1061
1061
1061
1062
1062
1062
1062
1063
1063
1063
1063
1064
1064
1064
1064
1065
1065
1065
1065
1066
1066
1066
1066
1067
1067
1067
1067
1068
1068
1068
1068
1069
1069
1069
1069
1070
1070
1070
1070
1071
1071
1071
1071
1072
1072
1072
1072
1073
1073
1073
1073
1074
1074
1074
1074
1075
1075
1075
1075
1076
1076
1076
1076
1077
1077
1077
1077
1078
1078
1078
1078
1079
1079
1079
1079
1080
1080
1080
1080
1081
1081
1081
1081
1082
1082
1082
1082
1083
1083
1083
1083
1084
1084
1084
1084
1085
1085
1085
1085
1086
1086
1086
1086
1087
1087
1087
1087
1088
1088
1088
1088
1089
1089
1089
1089
1090
1090
1090
1090
1091
1091
1091
1091
1092
1092
1092
1092
1093
1093
1093
1093
1094
1094
1094
1094
1095
1095
1095
1095
1096
1096
1096
1096
1097
1097
1097
1097
1098
1098
1098
1098
1099
1099
1099
1099
1100
1100
1100
1100
1101
1101
1101
1101
1102
1102
1102
1102
1103
1103
1103
1103
1104
1104
1104
1104
1105
1105
1105
1105
1106
1106
1106
1106
1107
1107
1107
1107
1108
1108
1108
1108
1109
1109
1109
1109
1110
1110
1110
1110
1111
1111
1111
1111
1112
1112
1112
1112
1113
1113
1113
1113
1114
1114
1114
1114
1115
1115
1115
1115
1116
1116
1116
1116
1117
1117
1117
1117
1118
1118
1118
1118
1119
1119
1119
1119
1120
1120
1120
1120
1121
1121
1121
1121
1122
1122
1122
1122
1123
1123
1123
1123
1124
1124
1124
1124
1125
1125
1125
1125
1126
1126
1126
1126
1127
1127
1127
1127
1128
1128
1128
1128
1129
1129
1129
1129
1130
1130
1130
1130
1131
1131
1131
1131
1132
1132
1132
1132
1133
1133
1133
1133
1134
1134
1134
1134
1135
1135
1135
1135
1136
1136
1136
1136
1137
1137
1137
1137
1138
1138
1138
1138
1139
1139
1139
1139
1140
1140
1140
1140
1141
1141
1141
1141
1142
1142
1142
1142
1143
1143
1143
1143
1144
1144
1144
1144
1145
1145
1145
1145
1146
1146
1146
1146
1147
1147
1147
1147
1148
1148
1148
1148
1149
1149
1149
1149
1150
1150
1150
1150
1151
1151
1151
1151
1152
1152
1152
1152
1153
1153
1153
1153
1154
1154
1154
1154
1155
1155
1155
1155
1156
1156
1156
1156
1157
1157
1157
1157
1158
1158
1158
1158
1159
1159
1159
1159
1160
1160
1160
1160
1161
1161
1161
1161
1162
1162
1162
1162
1163
1163
1163
1163
1164
1164
1164
1164
1165
1165
1165
1165
1166
1166
1166
1166
1167
1167
1167
1167
1168
1168
1168
1168
1169
1169
1169
1169
1170
1170
1170
1170
1171
1171
1171
1171
1172
1172
1172
1172
1173
1173
1173
1173
1174
1174
1174
1174
1175
1175
1175
1175
1176
1176
1176
1176
1177
1177
1177
1177
1178
1178
1178
1178
1179
1179
1179
1179
1180
1180
1180
1180
1181
1181
1181
```

IV. ARCHITECTURE RECOMMENDATION MODEL

To fully exploit the reconfigurability offered by the compute substrate, the best configuration needs to be identified depending on the workload. Identification of the best configuration, unfortunately can be a costly operation given the large size of the search space of possible configurations. For example, in Figure 8(a) we show the size of the configuration space of our flexible *systolic-cell* based architecture as a function of MAC units. A TPU v2 like system with 2^{14} MAC units has 858 possible configurations while a TPU v1 like system (2^{16} MAC units) has nearly 1400 configurations. For a given workload, configuration search over such large space at runtime can either be a performance bottleneck if implemented in a power limited system, or could end up using significant amount of energy as compared to the execution of the workload itself. In both the cases, this could undermine the benefits obtained from the flexible architecture system. Another alternative approach is to perform the search offline and store the configurations. However, this will only work when the workload configurations are known beforehand and are limited in size. For a data-center like use-case, where scaled systems are likely to be used, the variety of workloads is expected to be high. In this work we develop a novel technique to tackle this problem. Our solution is to replace the expensive search operation with a constant time neural network(NN) inference to procure the best configuration at runtime.

Search as a ML problem. The first step to design a constant time NN inference system is to pose the search problem to an ML problem. Out of the several alternative approaches, our experiments depicted posing the problem as a recommendation system, provided the best performance. The idea of a recommendation system is simple; when queried with the workload parameters (ie M, N, and K dimensions in our case) the network returns a category ID. This ID is used to a architecture configuration which provides the optimal performance for the workload. For our flexible *systolic-cell* based system the parameters captured by each category is depicted in Figure 8(b). As we depict in the figure, both the architecture configuration in terms of the systolic cell arrangements (first and second cols), systolic cell dimensions, as well as the mapping strategy is represented in terms of dataflow eg. output stationary (OS), weight stationary (WS), and input stationary (IS).

Recommendation Neural Network. We hand designed a recommendation system neural network. Given our use-case, there are two main requirements we need to satisfy. First, we need our network to have high accuracy in predicting the best runtime configuration which maximizes performance by attaining optimal mapping. Second, given that the recommendation network needs to be queried at runtime, the network should be small to lower costs. A smaller network will lead to low inference latency. In our use case, the recommendation inference for a given layer is run concurrent to the execution of a previous layer whenever possible. Lower inference latency therefore moves the recommendation step

out of the critical path. Moreover, smaller network has fewer computation and storage requirements therefore minimizing the overheads. Honoring these requirements, our proposed network is depicted in Figure 8(c). We use an embedding table to project the input features into a latent-space as in the DLRM and NCF models [12], [24]. The embedding lookups are then passed through two dense layers for classification, which chooses a category from the configuration space using softmax activation. We call this architecture ADAPTN. This simple model works very well for the flexible *systolic-cell* based arrays with different number of MAC units. Figure 8(d) depicts the accuracies obtained on test sets when the same model is trained to recommend configurations for varying number of MAC units. The model is trained for about 30 epoch on a separate datasets for each MAC units each containing about one million samples. We observe that the test accuracies are consistently over 90% and for a few configurations are as high as 96%. We also want to point out that the correct predictions correspond to the configuration which leads to the best runtime. Also it is germane to note that for the cases where the network recommends configurations other than the best possible ones, the performance is better than those we get in our baseline configurations (see Figure 9(c)). We distinguish the variants of this network by adding the number of categories as suffix. For example, the *systolic-cell* based SSA with 2^{14} MAC has 858 configurations, therefore the corresponding network is called ADAPTN-858.

V. SELF ADAPTIVE RECONFIGURABLE ARRAYS

By coupling ADAPTN with a reconfigurable array, we can create a self adaptive system which can be conceptually viewed as a combination of two units, a Self Adaptive unit (SA), and a Reconfigurable Array (RA) unit as shown in Figure 2. The SA unit encompasses the software and hardware components which recommend the optimal configurations. The RA unit is the hardware unit capable of flexibly configuring to the recommended configurations and hence run the workloads. It is worth pointing out that this design class is not specific to a reconfigurable core for running GEMM workloads. Instead any Coarse Grained Reconfigurable Array (CGRA) unit, configurable at runtime, can be augmented with a suitable SA, to ensure optimal performance. We believe this results in a new class of designs, which we name Self Adaptive Reconfigurable Array (SARA).

A. Hardware to run ADAPTN

In the context of our use case, an intuitive option is to allocate a few *systolic-cells* from the main array to run ADAPTN. However, this choice will lead to either fewer MAC units left for the actual workloads, or to allocate additional *systolic-cells* for ADAPTN leading to an additional overhead. An alternative to adding more *systolic-cells* will be to add a custom hardware dedicated for running ADAPTN. We explore both the *systolic-cell* and custom hardware options below. For the ease of discussion, we chose our RA to be a $1024 \times 4 \times 4$ *systolic-cell* unit (2^{14} MACs) which we call the SMARTSYSTOLIC unit.

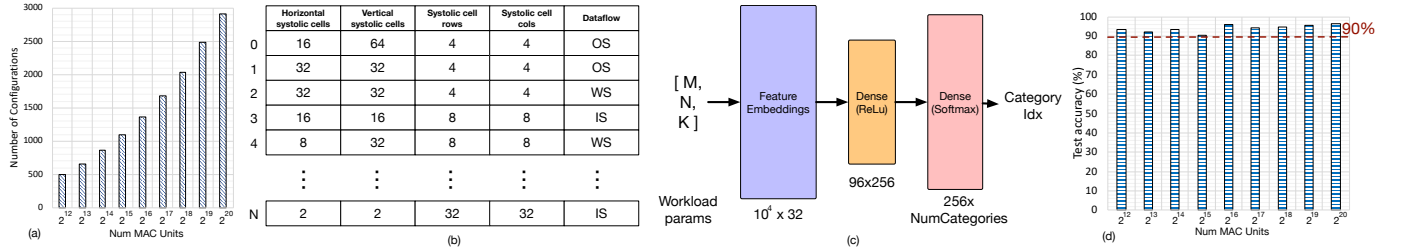


Fig. 8. (a) Size of the configuration space wrt number of MAC units for a *systolic-cell* based flexible array (b) Example of configurations predicted by ADAPTNET indexed by category ID (c) Schematic of the ADAPTNET topology (d) Test accuracies obtained on test sets for ADAPTNETs trained on *systolic-cell* based flexible array with various MAC units

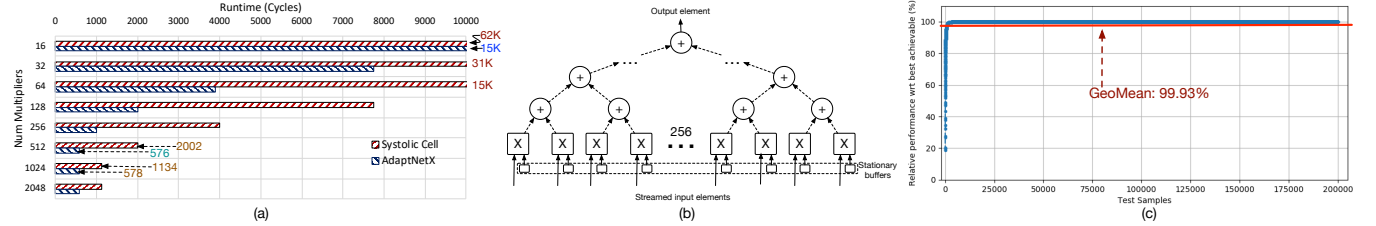


Fig. 9. (a) Cycles needed to run ADAPTNET-858 on an array of *systolic-cells* and on the custom hardware unit (ADAPTNETX) as a function of number of multipliers. (b) architecture of the custom 1-D unit hardware for ADAPTNETX(c) Relative performance of the configurations predicted by ADAPTNET-858 for SAGAR for 2×10^5 test samples when compared to the runtime of best possible configurations

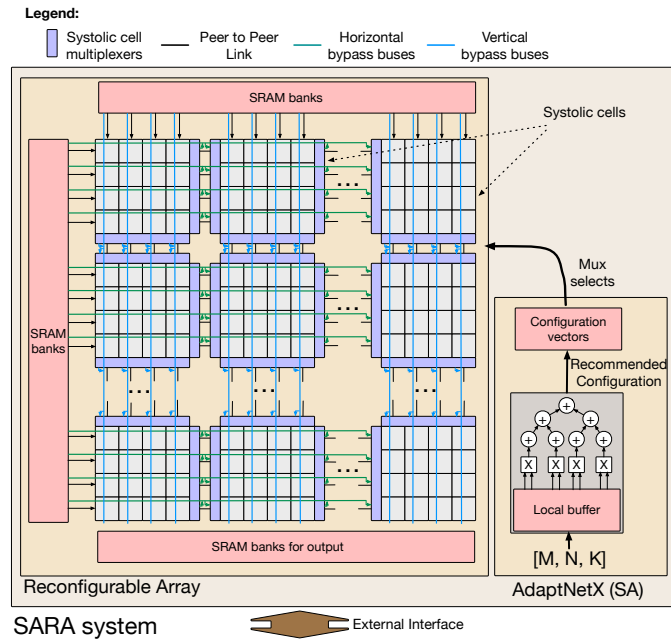


Fig. 10. Schematic of SAGAR, an instance of a SARA accelerator.

The corresponding recommendation that we use therefore is the ADAPTNET-858.

ADAPTNET Runtime on *systolic-cells*. Figure 9(a) shows the cycles required for a single inference of the ADAPTNET as a function of multipliers used in 4×4 *systolic-cell* based array. Understandably, the runtime decreases proportional to the increase in number of multipliers as we increase the number of *systolic-cells*, achieving the best runtime of 1134 cycles when using 1024 multipliers or 64 cells. When both the workloads and the recommendation engine is run on a same

array; for a TPU equivalent machine with 2^{14} MAC units, about 6.25% of the array needs to be allocated for running the ADAPTNET. Another choice could be allocating more hardware resources in terms of extra 64 *systolic-cells* dedicated to run the recommender network. However, given that ADAPTNET has exclusively dense layers processing the embedding lookups, a systolic execution turns out to be sub-optimal.

ADAPTNET Runtime on ADAPTNETX. We found a custom design tuned for ADAPTNET layer parameters to be more efficient. For efficient execution of the dense layers, we chose a 1-D multiplier unit with a binary tree based reduction as shown in Figure 9(b). We found Input stationary (IS) dataflow to be the most performant for our use case. In this mapping the elements of the input vector is buffered near the multipliers, while elements of the weight matrix are streamed through to generate one output element/partial sum, with a sustained throughput of 1 element per cycle. Throughput can be further increased by adding more such 1-D units. We name the custom core with one or more such 1-D units as ADAPTNETX. In Figure 9(a) we depict the variation of runtime of ADAPTNET inference on ADAPTNETX with two 1-D units as a function of multipliers. We find the 512 multipliers result in best runtime of 576 cycles, when running ADAPTNET for 2^{14} MAC unit *systolic-cell* design.

B. SAGAR Accelerator

SAGAR is constructed by augmenting the 2^{14} MAC SSA unit, laid out as 32×32 grid of *systolic-cells*, with ADAPTNETX running ADAPTNET-858 (see Figure 10). We chose this configuration as it has the same compute as the TPU v2, and the 4×4 *systolic-cell* size works the best for our workloads (see Section VI-A). Since each row and column in this configuration has 31 bypass links and one link to MAC,

TABLE I
Table depicting the architectural configuration of distributed systolic array based systems, monolithic systolic array baseline, and SAGAR

Name	Num Units	MAC/unit	Banks per SRAM buffer	Capacity per SRAM bank
Distributed 4x4 units (Baseline – GPU tensor core like)	1024	16	4	256 B
Distributed 8x8 units	256	64	8	512 B
Distributed 16x16 units	64	256	16	1 KB
Distributed 32x32 units	16	1024	32	2 KB
Distributed 64x64 units	4	4096	64	4 KB
Monolithic 128x128 (Baseline – TPU like)	1	16384	128	8 KB
SAGAR	1	16384	1024	1 KB

each buffer is constructed as a collection of 1024 1KB SRAM banks.

Real-time Reconfiguration. The ADAPTNETX uses an additional SRAM bank of 512KB to store the embedding table and the weight matrices for ADAPTNET-858. Each configuration corresponds to a 3968 bit vector which sets the bypass muxes, once the layer is ready to be mapped.

VI. EVALUATIONS

To showcase the capabilities of our proposed design, we evaluate *SAGAR* in two settings. To show the benefits that arise solely from the architecture aspects, we present results obtained from analysis done with a high level simulator. Then, to capture the implementation dependent aspects of the design, we implement *SAGAR* and the baselines in RTL and capture the PPA numbers by running Place-and-Route (PnR) flow. We also compare *SAGAR* with a state-of-the-art flexible accelerator architecture SIGMA [28]. The following subsections describe our findings in details.

A. Architectural evaluations

Methodology. For our architecture level studies we chose to use SCALE-Sim [33]. SCALE-Sim is a cycle accurate simulator for systolic array, which generates per cycle data accesses to and from various memories. This enables us to estimate and compare performance, energy consumption, power etc. of systolic array based components to a certain degree of accuracy. We created in-house scripts to generate SCALE-sim input files to perform the workload partitioning as generated by ADAPTNET-858.

Workloads. For our evaluations we choose FasterRCNN [29], DeepSpeech2 [2], and AlphaGoZero [36], as our workloads as a representative of convolution neural networks, language modelling network, and DNNs for reinforcement learning respectively.

Baselines. We have two baselines, a large monolithic systolic array and a collection of small systolic arrays to work as a single distributed system (see Table I). We modelled the monolithic systolic array with the same dimensions as Google’s TPU v2, with 128×128 MAC units. However unlike TPU v2 which supports floating point MAC operations, our model assumes byte long words, which is the accepted size for operands for inference operations. We allocated a total 3MB of SRAM memory to the entire array divided into 3 operand buffers, one for each input operand matrix and the output matrix. Although

TABLE II
Dimensions for the synthetic GEMM workloads

	G1	G2	G3	G4	G5	G6	G7	G8	G9	G10
M	128	256	512	1024	2048	128	256	512	1024	2048
K	128	256	512	1024	2048	64	64	64	64	64
N	128	256	512	1024	2048	64	64	64	64	64
	G11	G12	G13	G14	G15	G16	G17	G18	G19	G20
M	64	64	64	64	64	64	64	64	64	64
K	64	64	64	64	64	128	256	512	1024	2048
N	128	256	512	1024	2048	64	64	64	64	64

we would like to point out that, SCALE-Sim assumes that there is sufficient DRAM bandwidth available for ideal prefetching of operands, and therefore the computation runs in a stall free mode. Therefore, for runtime generated by simulation the SRAM sizes have no impact. Nevertheless, previous work [33] has shown that buffer sizes of this scale lead to reasonable off-chips requests.

For our second baseline, we chose a collection of 4×4 systolic arrays. This choice is motivated by the sizes of the Nvidia tensor cores, which are small matrix multiplication units available as special functional units Nvidia’s GPUs from their Volta architecture onward. Although the largest data-center GPUs have 84 streaming multiprocessors [25] per unit, we choose a collection of 1024 such 4×4 array as our system, to keep the compute capability of both our baselines the same. We also keep the total amount of memory in the system equal to the monolithic baseline. The buffer size of each individual array is determined by uniformly dividing each corresponding individual buffer size in the monolithic array.

Performance Analysis. We model both of the baseline systems and *SAGAR* in SCALE-Sim and compare the performance for our workloads. In Figure 11(a) we depict the cycles taken to run all the layers in AlphaGoZero, DeepSpeech2, and the first 10 layers of FasterRCNN networks. Among the baselines, the distributed configuration mostly results in faster runtime owing to higher mapping flexibility. However *SAGAR*, owing to reconfigurability is capable of matching the better baseline configuration. Naturally, this flexibility leads to lower aggregated runtime for *SAGAR* than either of the baselines.

Favorable Configurations. *SAGAR* is also capable of realizing configurations which are out of scope of either of baselines. This allows *SAGAR* to achieve higher performance than both the baselines on certain layers. For example, consider the synthetic GEMM operands depicted in Table II. Figure 12(a) depicts the histogram of the best configuration for these layers obtained from simulation. The layers favouring 8×8 or 32×32 configurations constitute about 40% of the set. Neither of these configurations can be realized a fixed array configuration like the baselines. In Figure 12(b,c,d) we show the histogram of a similar experiment conducted on our DNN workloads. For these specific workloads, the 4×4 configuration works the best for majority of the layers. This observation also explains our findings in Figure 11(a) on why *SAGAR*’s performance is identical to the 4×4 baseline. Nevertheless, for layers which favor configurations like 8×8 , 32×32 etc. *SAGAR* will lead to lower runtime than both the baselines. This is depicted by Figure 11(c), where we see that *SAGAR* achieves about $> 10 \times$

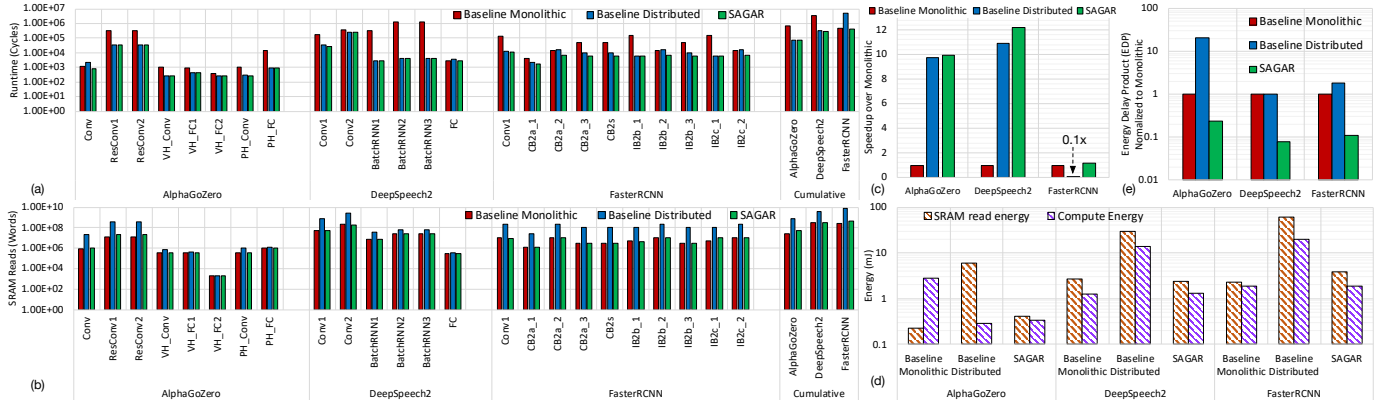


Fig. 11. (a) Simulated runtimes for monolithic 128×128 baseline, distributed $1024 \times 4 \times 4$ baseline, and SAGAR for layers in AlphaGoZero, DeepSpeech2, and first 10 layers of FasterRCNN (b) SRAM reads for the same workloads for SAGAR and baseline configurations (c) Speedup of SAGAR and distributed baseline as compared to the monolithic baseline (d) Energy consumption breakdown for our workloads in SAGAR and baselines (e) Energy delay product(EDP) of SAGAR and baselines, normalized to EDP for monolithic baseline

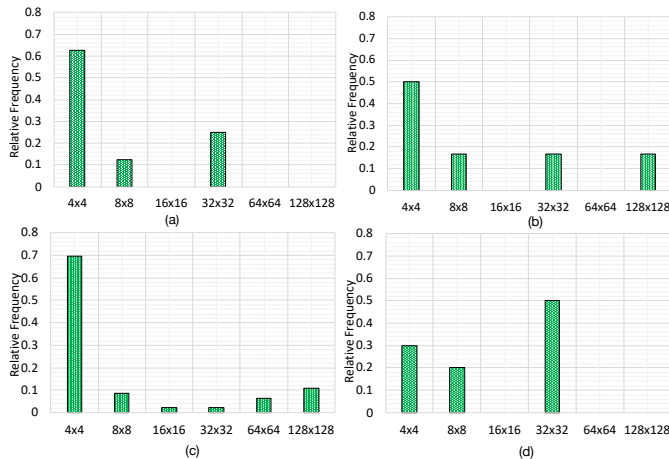


Fig. 12. Distribution of favorable array sizes for a 16384 MAC distributed system which attain the lowest runtime when run for each layer in (a) synthetic GEMM workloads (b) AlphaGoZero, (c) DeepSpeech2, and (d) FasterRCNN.

speedup over monolithic when distributed configurations are preferred. While in cases where monolithic is preferred it runs faster than both the baselines.

SRAM reads and Energy efficiency. In designs where a large number of computations are executed in parallel, reducing the number of SRAM reads can lead to a high energy savings given it does not negatively influence performance. In general, due to the loss of reuse, distributed configurations with smaller array sizes have more SRAM reads. We observe this trend in action in Figure 11(b) where we depict the number of SRAM reads performed for layers when running our workloads on the two baselines and on SAGAR. The distributed 4×4 system has much higher number of reads as compared to SAGAR and the monolithic baseline. In SAGAR this efficiency loss in reuse is mitigated by using bypassing links. As shown in Figure 11(b), across all layers in our workloads, SAGAR incurs SRAM reads close to that in the monolithic baseline. In the case of DeepSpeech2, SAGAR, owing to efficient mapping, incurs reads even fewer than that of the monolithic baseline.

To further quantify the efficiency of SAGAR, we estimated the energy spent by the three configurations on the workloads by taking into the cycle counts and the SRAM reads and scaling the counts by typical energy consumed per operation computed from RTL PnR flows. In Figure 11(d) we plot the energy consumed normalized to the energy of the monolithic array. We observe that for workloads amenable to monolithic array (ie. FasterRCNN and DeepSpeech2), SAGAR's energy consumption is almost identical to the monolithic baseline. The distributed baseline on the other hand consumes an order of magnitude higher energy for all the three workloads, while supporting the same mapping configurations as SAGAR. For AlphaGoZero, which favours a distributed configuration, SAGAR consumes about 20% of the energy consumed by the monolithic baseline, while almost one order of magnitude lower than that of the distributed baseline. Figure 11(d) also shows that SAGAR's energy consumption for SRAM is close to that of consumed by the monolithic array for all the three workloads. The computation energy consumption in SAGAR equivalent to the better of the two baselines. The combined effect of improved latency and reuse is perhaps better represented by the energy-delay product (EDP) depicted by Figure 11(e). In this figure we plot the EDP for SAGAR and the two baselines normalized to the values corresponding to the monolithic configuration. We observe that SAGAR results in about 92% to 80% less EDP compared to the monolithic baseline. This further demonstrates the efficiency of our proposed architecture, resulting from preserving reuse while simultaneously decreasing latency due to improved mapping.

B. Implementation evaluations

Methodology. We implemented SAGAR in RTL and as a 32×32 array of 4×4 *systolic-cells* and ran ASIC flow till Place-and-Route (PnR) to obtain area and power. We used 28nm library for implementing the logic. We also implemented the SRAM buffers as a collection of 1024 1KB cells with the SAED32 education library from Synopsis, to quantify the power and area overheads, and then scaled down to 28nm

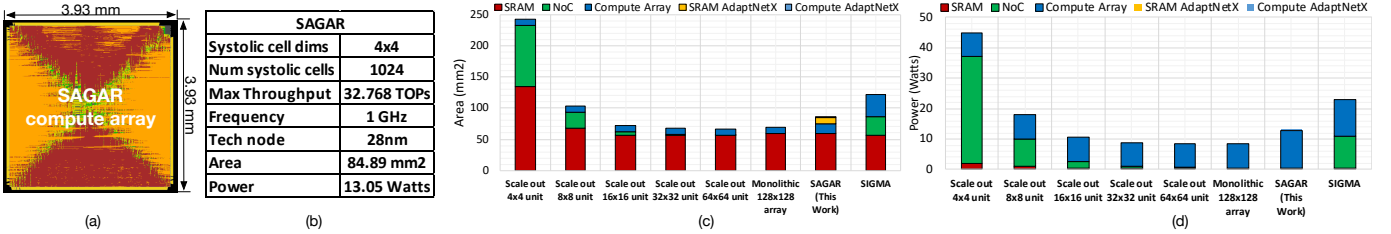


Fig. 13. (a) The post PnR floor-plan diagram of SAGAR’s compute array, (b) A table detailing architecture configuration of SAGAR, the implementation parameters, and post PnR area and power of SAGAR. (c) The comparison and breakdown of post synthesis area for distributed systolic array based designs, the monolithic systolic baseline, SAGAR, and SIGMA (d) The corresponding breakdown for power consumed by various components in distributed systolic array based designs, the monolithic systolic baseline, SAGAR, and SIGMA

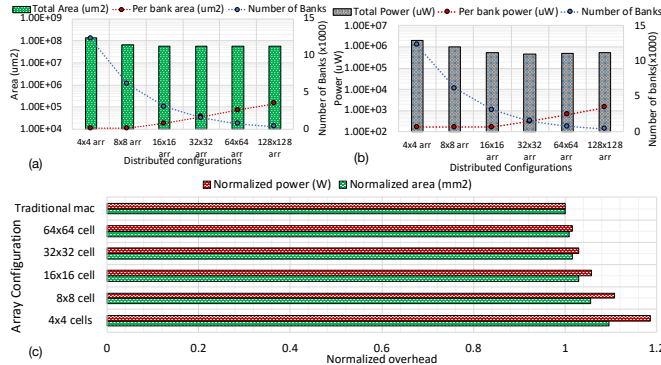


Fig. 14. (a) The variation of total area footprint of SRAM banks in various distributed systolic array and monolithic configuration juxtaposed with the variation in bank sizes and the number of banks required, (b) A similar variation in the power consumption by the SRAM banks in distributed systolic array and monolithic configurations, and (c) the the area and power of a 128×128 array when constructed using different sized of “systolic-cells” normalized to the area and power of an array constructed with traditional MAC units.

equivalent by using Dennard’s scaling [6]. Figure 13(a) depicts the post PnR floorplan of SAGAR’s compute logic. Figure 13(b) lists the array configuration, area, and power consumption reported after PnR by synthesizing the SSA and memory at a operating frequency of 1 GHz. At 32.768 TOPs (with 1 MAC being two operation) at 1 GHz SAGAR takes 84.89 mm^2 of real estate while consuming 13.05 Watts of power. The ADAPTNEX consumes 12.4% of total area and 1.6% of total power.

Baselines. We implement the baseline monolithic 128×128 systolic array and distributed 4×4 array in RTL. The distributed array is implemented using 1024 identical 4×4 traditional systolic arrays connected together by a mesh interconnect. We used the OpenSMART [19] tool to generate and synthesize the mesh topologies for these systems.

The total memory capacity of both the monolithic and the distributed configurations are kept the same at 3MB. As discussed in Section VI-A the monolithic array has two input operand buffer of 1MB each and an output buffer also with the 1MB capacity. In our implementation, we opted for one bank per row or column of the array. This choice ensures that each incoming link to the array will have full bandwidth from SRAM provided that bank conflicts are negligible. Therefore

each buffer in the monolithic baseline is constructed using 128, 8KB banks. For the distributed configuration, for each 4×4 array we end up with 1MB for each operand buffer. Using the same design approach as above, we end up with each buffer being constructed using 4 banks of 256 words each. In Table I we extend the same design principle for designing the memory for various other cell sizes and for SAGAR. In SAGAR, in addition to the links going directly from the SRAM to the edge MAC units of the array, we have to consider the bypass links as well. To get full bandwidth on these links we need to consider additional buffers. Extending the design described in Figure 6, each row and column of SAGAR has 31 bypass links and one link to the first MAC unit, we need 32 banks per row/column. Therefore each SRAM buffer is constructed with 1024, 1KB banks.

Area Analysis. In Figure 13(c) we depict the break down of area overheads for SRAM buffers, mesh NoC, and the compute array for various distributed configurations, the monolithic array, SAGAR and SIGMA [28]. We observe that the monolithic configuration is the most efficient in terms of area, where it is about $5 \times$ more compact than the distributed 4×4 array configuration. The breakdown suggests that the bloating in the distributed 4×4 configuration is caused predominantly by the Mesh NoC (contributing to 40.5%), followed by the SRAM buffers. SAGAR on the other hand takes about 8% more area than the monolithic array, while consuming about $3.2 \times$ lower area than the distributed 4×4 configuration. Considering both SAGAR and the distributed configuration provides same mapping flexibility, the proposed design is strictly more efficient. SAGAR is also more compact than SIGMA, taking about 70% of the area while packing equal number of compute units.

Across the various systolic-array configurations in Figure 13(c), the SRAM area appears to remain fairly constant. This is a direct consequence of the buffer capacity and construction of the array. In Figure 14(a) we depict the total area obtained for various configurations depicted in Table I. We observe that, the various configurations vary in the bank capacity and the number of banks. Since the total capacity remains the same across the configurations, these factor counter balance each other leading to observed trends.

Power Consumption. In Figure 13(d) we depict the post PnR power consumption for various array configuration. The

Mesh NoC stands out as the major contributor, which naturally makes the 4×4 distributed configuration about $5.3 \times$ more expensive than the monolithic configuration, with the NoC contributing to about 78% of the power. Considering the power of the compute array alone, all the systolic-array based configurations appear to consume similar power. We also depict the trend in power consumed by SRAM banks across various systolic-array based configurations in Figure 14(b). Similar to the trends observed in area breakdown, the counter balancing affects of increasing the bank sizes and lowering of number of banks lead to similar powers across various distributed and monolithic configurations.

SSA however consumes about 50% more power than the monolithic configuration, owing to the bypass links. However this extra cost results in achieving the same mapping flexibility of the 4×4 distributed configuration, which is about $3.5 \times$ more expensive. *SAGAR therefore is almost as scalable as a native monolithic systolic array in terms of area, while consuming about 50% more power, it provides the same mapping flexibility and performance as a distributed scaled out configuration using 4×4 systolic arrays.* Furthermore, SAGAR consumes about 43% less power than SIGMA, owing to the relatively simple interconnection network.

To explore further opportunities for optimization in SAGAR's implementation, in Figure 14(c) we plot the area and power of the compute array for varying systolic cell sizes, normalized to the area/power of the monolithic configuration. It is evident that both the power and area overheads increase by decreasing the cell sizes. Using larger cells might be tempting, but it comes at the cost of mapping flexibility. As depicted in Figure 12(b,c,d), our workloads predominantly favour 4×4 cells. However, for specialized use-cases which favor larger cell sizes (eg. Figure 12(a)) cheaper implementation is possible.

Summary. *Considering our findings from architectural simulations and physical implementation, we conclude that the proposed Self Adaptive Reconfigurable hardware enables achieving both high performance and energy efficiency simultaneously. The SMARTSYSTOLIC compute unit enables high mapping efficiency of a fine-grained flexible architecture, while retaining the scalability of monolithic systolic array. The novel ADAPTNET ensures optimal configuration at runtime with high accuracy, while minimizing performance, power, and area overheads when run on the proposed ADAPTNEX.*

VII. RELATED WORKS

Flexible DNN Accelerator. To efficiently execute a variety of workloads, DNN accelerator designs generally come with two tiers of flexibility, architecture and dataflow. Designs like Neurocube [16], Flexflow [22], and by FPGA based designs [37] enable flexible mapping by supporting multiple dataflow. On the other hand proposals like Planaria [10], Brainwave [7], SIGMA [28], MAERI [20], Cascades [31] and others [1], [9], [37] enable reconfiguration at the hardware level for efficient execution. The SMARTSYSTOLIC array in SAGAR enables both mapping flexibility and reconfigurability. Table III depicts the standing of various such accelerators in term of native operation supported, mapping capability and flexibility.

TABLE III

Table depicting previous accelerator proposals categorized in terms of computation support, mapping capability, and flexibility offered in term of hardware reconfiguration or dataflow supported

	Native Operation	Mapping	Capability	Flexibility		
	Convolution	GEMM	Homogenous	Heterogenous	Dataflow	Architecture
Zhang et al. [37]	✓		✓		✓	✓
Eyeriss [4]	✓		✓			
Alwani et al. [1]	✓			✓		✓
NeuroCube [16]	✓			✓	✓	
MAERI [20]	✓		✓	✓		✓
TPU [13]		✓	✓		✓	
Flexflow [22]	✓		✓		✓	
Tetris [8]	✓			✓		
Brainwave [7]		✓	✓			✓
Simba [35]		✓		✓		
Tangram [9]	✓			✓		
Cascades [31]	✓			✓		✓
Sigma [28]		✓		✓		✓
Planaria [10]	✓		✓		✓	
SAGAR (This work)	✓	✓	✓	✓	✓	✓

Dataflow and Accelerator Design Space Search. Several architecture and mapping space exploration tools have been proposed in the recent past to take advantage of flexibilities in the design. Tool like SCALE-Sim [32], MAESTRO [18], Tetris [8] etc. provide analytical models for fast cost estimation of specific configurations. While Timeloop [27], dMazeRunner [5] etc are tools which perform heuristic or exhaustive search for architecture configuration or mapping strategy. SARA systems like SAGAR on the other hand use a trained recommender like ADAPTNET to circumvent the search and obtain the optimal configuration and dataflow in one shot at runtime.

ML assisted system configuration. Recent works have demonstrated the use of ML algorithms to assist in system configuration. Gamma [15] and Confuciux [14] perform architecture mapping and design space configuration search using genetic algorithm and reinforcement learning (RL). On more systems size, work by Mirhoseni et al [23] use RL for task placement on a heterogenous system, while modern compilers like AutoTVM [3] use ML models for cost prediction to improve compilation time. Nautilus [26] uses genetic algorithm to improve FPGA place and route. It is worth noting that these approaches mostly enhance search for the optimal configuration, and this unlike ADAPTNET do not replace search. Perhaps the closest to our approach is work by Kwon et al [21], who use online tensor-based recommender systems to aid place and route in chip design.

VIII. CONCLUSIONS

In this paper we present a new class of accelerators named *Self Adaptive Reconfigurable Arrays* (SARA). We develop SARA by augmenting a reconfigurable array with a hardware running a neural network recommender system. The recommender system can provide optimal configuration of the array at runtime when as the workload arrives. This makes the array self sufficient to run optimally. We design a novel, highly accurate and fast recommendation network called ADAPTNET, and a specialized hardware accelerator ADAPTNEX. We also present a new design approach for building scalable GEMM accelerator architectures by augmenting traditional systolic array units with SMART [17]-like bypass links called 'systolic-

cells'. This SMARTSYSTOLIC array can be configured to operate in any regime between a monolithic *scaled-up* and distributed *scaled-out* architecture. Using a reference design named *SAGAR*, we show that we can simultaneously achieve high mapping flexibility and exploit spatio-temporal reuse, therefore achieving both performance and energy efficiency.

REFERENCES

- [1] M. Alwani, H. Chen, M. Ferdman, and P. Milder, "Fused-layer cnn accelerators," in *2016 49th Annual IEEE/ACM International Symposium on Microarchitecture (MICRO)*. IEEE, 2016, pp. 1–12.
- [2] D. Amodei, S. Ananthanarayanan, R. Anubhai, J. Bai, E. Battenberg, C. Case, J. Casper, B. Catanzaro, Q. Cheng, G. Chen *et al.*, "Deep speech 2: End-to-end speech recognition in english and mandarin," in *International conference on machine learning*, 2016, pp. 173–182.
- [3] T. Chen, L. Zheng, E. Yan, Z. Jiang, T. Moreau, L. Ceze, C. Guestrin, and A. Krishnamurthy, "Learning to optimize tensor programs," in *Advances in Neural Information Processing Systems*, 2018, pp. 3389–3400.
- [4] Y.-H. Chen, J. Emer, and V. Sze, "Eyeriss: A spatial architecture for energy-efficient dataflow for convolutional neural networks," *ACM SIGARCH Computer Architecture News*, vol. 44, no. 3, pp. 367–379, 2016.
- [5] S. Dave, Y. Kim, S. Avancha, K. Lee, and A. Shrivastava, "Dmazerunner: Executing perfectly nested loops on dataflow accelerators," *ACM Transactions on Embedded Computing Systems (TECS)*, vol. 18, no. 5s, pp. 1–27, 2019.
- [6] R. H. Dennard, F. H. Gaensslen, V. L. Rideout, E. Bassous, and A. R. LeBlanc, "Design of ion-implanted mosfet's with very small physical dimensions," *IEEE Journal of Solid-State Circuits*, vol. 9, no. 5, pp. 256–268, 1974.
- [7] J. Fowers, K. Ovtcharov, M. Papamichael, T. Massengill, M. Liu, D. Lo, S. Alkalay, M. Haselman, L. Adams, M. Ghandi *et al.*, "A configurable cloud-scale dnn processor for real-time ai," in *2018 ACM/IEEE 45th Annual International Symposium on Computer Architecture (ISCA)*. IEEE, 2018, pp. 1–14.
- [8] M. Gao, J. Pu, X. Yang, M. Horowitz, and C. Kozyrakis, "Tetris: Scalable and efficient neural network acceleration with 3d memory," in *Proceedings of the Twenty-Second International Conference on Architectural Support for Programming Languages and Operating Systems*, 2017, pp. 751–764.
- [9] M. Gao, X. Yang, J. Pu, M. Horowitz, and C. Kozyrakis, "Tangram: Optimized coarse-grained dataflow for scalable nn accelerators," in *Proceedings of the Twenty-Fourth International Conference on Architectural Support for Programming Languages and Operating Systems*, 2019, pp. 807–820.
- [10] S. Ghodrati, B. H. Ahn, J. K. Kim, S. Kinzer, B. R. Yatham, N. Alla, H. Sharma, M. Alian, E. Ebrahimi, N. S. Kim *et al.*, "Planaria: Dynamic architecture fission for spatial multi-tenant acceleration of deep neural networks," in *2020 53rd Annual IEEE/ACM International Symposium on Microarchitecture (MICRO)*. IEEE, 2020, pp. 681–697.
- [11] X. He and T.-S. Chua, "Neural factorization machines for sparse predictive analytics," in *Proceedings of the 40th International ACM SIGIR conference on Research and Development in Information Retrieval*, 2017, pp. 355–364.
- [12] X. He, L. Liao, H. Zhang, L. Nie, X. Hu, and T.-S. Chua, "Neural collaborative filtering," in *Proceedings of the 26th international conference on world wide web*, 2017, pp. 173–182.
- [13] N. P. Jouppi, C. Young, N. Patil, D. Patterson, G. Agrawal, R. Bajwa, S. Bates, S. Bhatia, N. Boden, A. Borchers *et al.*, "In-datacenter performance analysis of a tensor processing unit," in *Proceedings of the 44th Annual International Symposium on Computer Architecture*, 2017, pp. 1–12.
- [14] S.-C. Kao, G. Jeong, and T. Krishna, "Confuciux: Autonomous hardware resource assignment for dnn accelerators using reinforcement learning," in *2020 53rd Annual IEEE/ACM International Symposium on Microarchitecture (MICRO)*. IEEE, 2020, pp. 622–636.
- [15] S.-C. Kao and T. Krishna, "Gamma: Automating the hw mapping of dnn models on accelerators via genetic algorithm," in *ICCAD*, 2020.
- [16] D. Kim, J. Kung, S. Chai, S. Yalamanchili, and S. Mukhopadhyay, "Neurocube: A programmable digital neuromorphic architecture with high-density 3d memory," *ACM SIGARCH Computer Architecture News*, vol. 44, no. 3, pp. 380–392, 2016.
- [17] T. Krishna, C.-H. O. Chen, W.-C. Kwon, and L.-S. Peh, "Smart: single-cycle multi-hop traversals over a shared network on chip," *IEEE micro*, vol. 34, no. 3, pp. 43–56, 2014.
- [18] H. Kwon, P. Chatarasi, M. Pellauer, A. Parashar, V. Sarkar, and T. Krishna, "Understanding reuse, performance, and hardware cost of dnn dataflow: A data-centric approach," in *Proceedings of the 52nd Annual IEEE/ACM International Symposium on Microarchitecture*, 2019, pp. 754–768.
- [19] H. Kwon and T. Krishna, "Opensmart: Single-cycle multi-hop noc generator in bsv and chisel," in *2017 IEEE International Symposium on Performance Analysis of Systems and Software (ISPASS)*. IEEE, 2017, pp. 195–204.
- [20] H. Kwon, A. Samajdar, and T. Krishna, "Maeri: Enabling flexible dataflow mapping over dnn accelerators via reconfigurable interconnects," *ACM SIGPLAN Notices*, vol. 53, no. 2, pp. 461–475, 2018.
- [21] J. Kwon, M. M. Ziegler, and L. P. Carloni, "A learning-based recommender system for autotuning design flows of industrial high-performance processors," in *2019 56th ACM/IEEE Design Automation Conference (DAC)*. IEEE, 2019, pp. 1–6.
- [22] W. Lu, G. Yan, J. Li, S. Gong, Y. Han, and X. Li, "Flexflow: A flexible dataflow accelerator architecture for convolutional neural networks," in *2017 IEEE International Symposium on High Performance Computer Architecture (HPCA)*. IEEE, 2017, pp. 553–564.
- [23] A. Mirhoseini, H. Pham, Q. V. Le, B. Steiner, R. Larsen, Y. Zhou, N. Kumar, M. Norouzi, S. Bengio, and J. Dean, "Device placement optimization with reinforcement learning," *arXiv preprint arXiv:1706.04972*, 2017.
- [24] M. Naumov, D. Mudigere, H.-J. M. Shi, J. Huang, N. Sundaraman, J. Park, X. Wang, U. Gupta, C.-J. Wu, A. G. Azzolini *et al.*, "Deep learning recommendation model for personalization and recommendation systems," *arXiv preprint arXiv:1906.00091*, 2019.
- [25] T. NVIDIA, "Nvidia tesla v100 gpu architecture," <https://images.nvidia.com/content/volta-architecture/pdf/volta-architecture-whitepaper.pdf>, 2017.
- [26] M. K. Papamichael, P. Milder, and J. C. Hoe, "Nautilus: Fast automated ip design space search using guided genetic algorithms," in *Proceedings of the 52nd Annual Design Automation Conference*, 2015, pp. 1–6.
- [27] A. Parashar, P. Raina, Y. S. Shao, Y.-H. Chen, V. A. Ying, A. Mukkara, R. Venkatesan, B. Khailany, S. W. Keckler, and J. Emer, "Timeloop: A systematic approach to dnn accelerator evaluation," in *2019 IEEE international symposium on performance analysis of systems and software (ISPASS)*. IEEE, 2019, pp. 304–315.
- [28] E. Qin, A. Samajdar, H. Kwon, V. Nadella, S. Srinivasan, D. Das, B. Kaul, and T. Krishna, "Sigma: A sparse and irregular gemm accelerator with flexible interconnects for dnn training," in *2020 IEEE International Symposium on High Performance Computer Architecture (HPCA)*, 2020.
- [29] S. Ren, K. He, R. Girshick, and J. Sun, "Faster r-cnn: Towards real-time object detection with region proposal networks," in *Advances in neural information processing systems*, 2015, pp. 91–99.
- [30] S. Rendle, "Factorization machines," in *2010 IEEE International Conference on Data Mining*. IEEE, 2010, pp. 995–1000.
- [31] A. Samajdar, T. Garg, T. Krishna, and N. Kapre, "Scaling the cascades: Interconnect-aware fpga implementation of machine learning problems," in *2019 29th International Conference on Field Programmable Logic and Applications (FPL)*. IEEE, 2019, pp. 342–349.
- [32] A. Samajdar, J. M. Joseph, Y. Zhu, P. Whatmough, M. Mattina, and T. Krishna, "A systematic methodology for characterizing scalability of dnn accelerators using scale-sim," in *2020 IEEE International Symposium on Performance Analysis of Systems and Software (ISPASS)*, 2020.
- [33] A. Samajdar, Y. Zhu, P. Whatmough, M. Mattina, and T. Krishna, "Scale-sim: Systolic cnn accelerator simulator," *arXiv preprint arXiv:1811.02883*, 2018.
- [34] B. Sarwar, G. Karypis, J. Konstan, and J. Riedl, "Item-based collaborative filtering recommendation algorithms," in *Proceedings of the 10th international conference on World Wide Web*, 2001, pp. 285–295.
- [35] Y. S. Shao, J. Clemons, R. Venkatesan, B. Zimmer, M. Fojtik, N. Jiang, B. Keller, A. Klinefelter, N. Pinckney, P. Raina *et al.*, "Simba: Scaling deep-learning inference with multi-chip-module-based architecture," in *Proceedings of the 52nd Annual IEEE/ACM International Symposium on Microarchitecture*, 2019, pp. 14–27.
- [36] D. Silver, J. Schrittwieser, K. Simonyan, I. Antonoglou, A. Huang, A. Guez, T. Hubert, L. Baker, M. Lai, A. Bolton *et al.*, "Mastering the game of go without human knowledge," *Nature*, vol. 550, no. 7676, pp. 354–359, 2017.

[37] C. Zhang, P. Li, G. Sun, Y. Guan, B. Xiao, and J. Cong, “Optimizing fpga-based accelerator design for deep convolutional neural networks,” in *Proceedings of the 2015 ACM/SIGDA International Symposium on Field-Programmable Gate Arrays*, 2015, pp. 161–170.